

Long-time dynamics of quantum chains: transfer-matrix renormalization group and entanglement of the maximal eigenvector

Yu-Kun Huang,^{1,*} Pochung Chen,^{2,†} Ying-Jer Kao,^{3,‡} and Tao Xiang^{4,§}

¹Graduate School of Engineering Science and Technology,

Nan Jeon University of Science and Technology, Tainan 73746, Taiwan

²Department of Physics and Frontier Research Center on Fundamental and Applied Sciences of Matters,
National Tsing Hua University, Hsinchu 30013, Taiwan

³Department of Physics and Center for Advanced Study of Theoretical Science,
National Taiwan University, No. 1, Sec. 4, Roosevelt Rd., Taipei 10607, Taiwan

⁴Institute of Physics, Chinese Academy of Sciences, P.O. Box 603, Beijing 100190, China
(Dated: May 30, 2018)

By using a different quantum-to-classical mapping from the Trotter-Suzuki decomposition, we identify the entanglement structure of the maximal eigenvectors for the associated quantum transfer matrix. This observation provides a deeper insight into the problem of linear growth of the entanglement entropy in time evolution using conventional methods. Based on this observation, we propose a general method for arbitrary temperatures using the biorthonormal transfer-matrix renormalization group. Our method exhibits a competitive accuracy with a much cheaper computational cost in comparison with two recent proposed methods for long-time dynamics based on a folding algorithm [Phys. Rev. Lett. **102**, 240603 (2009)] and a modified time-dependent density-matrix renormalization group [Phys. Rev. Lett. **108**, 227206 (2012)].

PACS numbers: 03.67.Mn, 02.70.-c, 75.10.Jm

The response function of a system subject to an external perturbation is a fundamental quantity to understand the mechanism inside a strongly interacting system. In particular, the time-dependent correlation function, whose Fourier transformation gives the spectral information about the system, can be measured in experiments. Therefore, it is important to be able to study the time-dependent correlation function with high accuracy. For one-dimensional (1D) systems, the density matrix renormalization group (DMRG) is an efficient algorithm to accurately obtain the ground state of interacting quantum models[1], and has been extended to address real-time dynamics [2] and the computation of thermodynamic quantities[3]. Long-time dynamics, however, remains difficult due to the linear growth of the entanglement entropy as the state evolves in time[3, 4]. Recently, two schemes have been proposed which allow numerical stable computation of the long-time dynamics. The folding scheme uses a more efficient representation of the entanglement structure in the tensor network obtained from the Trotter-Suzuki decomposition, by folding the network in the time direction prior to contraction[5]. On the other hand, a modified finite-temperature time-dependent DMRG (tDMRG) scheme exploits the freedom of applying unitary transformations in the ancilla space [6]. Although these methods can reach longer time scale than before, it is not clear the reason why they should work and whether if they can be extended to generic quantum models.

In this paper, we construct a single-site quantum transfer matrix (QTM) using an alternative quantum-to-classical mapping[7] for generic quantum models. Analyzing this QTM gives us a clear picture of the entan-

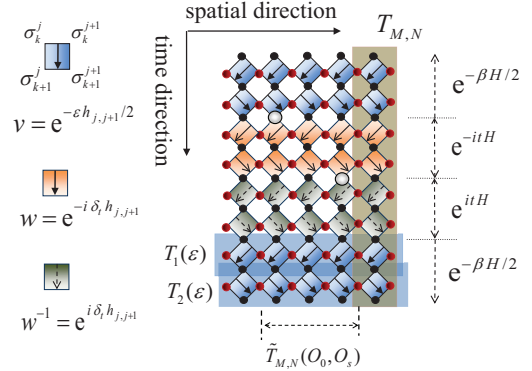


FIG. 1. (Color online) Graphical representation of the evolution matrices $T_{1,2}(\epsilon)$ and the quantum transfer matrix $T_{M,N}$. σ_k^j is a basis state at site j and time (or imaginary time) k . $\tilde{T}_{M,N}(O_0, O_s)$ is a product of $s + 1$ transfer matrices where the two empty circles represents two operators at different site and different time. Detailed definitions of these matrices are given in Supplementary Material S1.

glement structure for the QTM. This not only provides a deeper insight into the problem of entanglement growth during the time evolution, but also a heuristic argument on why the conventional schemes break down at long time scale and why the folding and the modified tDMRG schemes work. Furthermore, we propose an alternative scheme using the biorthonormal transfer-matrix DMRG (BTMRG) [8] by partitioning the QTM into system and environment blocks according to the entanglement structure. We show that our scheme exhibits the same level of accuracy with a much cheaper numerical cost.

We start from a 1D quantum system with L sites and

a Hamiltonian $H = \sum_{j=1}^L h_{j,j+1}$ with nearest-neighbor interactions and periodic boundary conditions. The time dependent correlation function for an operator O between site s and site 0 at finite temperature can be expressed as

$$\langle O_s(t)O_0(0) \rangle = \frac{1}{Z} \text{Tr} \left(e^{-\beta H} e^{itH} O_s e^{-itH} O_0 \right), \quad (1)$$

where $Z = \text{Tr}(e^{-\beta H})$ is the partition function and $\beta = 1/T$ is the inverse temperature.

We employ a quantum-to-classical mapping that decomposes the operator $e^{-\beta H}$ into

$$e^{-\beta H} \approx \lim_{M \rightarrow \infty} [T_1(\varepsilon) T_2(\varepsilon)]^{M/2}, \quad (2)$$

where $T_{1,2}(\varepsilon) = T_{R,L} e^{-\varepsilon H}$ is a row-to-row evolution operator, and $T_{R,L}$ are the right and left shift operators which are defined by the product of a 45° clockwise and counter-clockwise rotated local operator $\nu \equiv e^{-\varepsilon h_{j,j+1}}$, respectively. $\varepsilon = \beta/M$ is the imaginary-time step and M is the Trotter number in the imaginary-time direction [7]. A similar decomposition can be applied to the operators e^{-itH} and e^{itH} by replacing ν with the complex local operators $w \equiv e^{-i\delta_t h_{j,j+1}}$ and $w^{-1} \equiv e^{i\delta_t h_{j,j+1}}$, respectively. Here $\delta_t = t/N$ and N is the Trotter number in the time direction. From these decompositions a column-to-column QTM, $T_{M,N}$, can be defined. A graphical representation of $T_{M,N}$ is shown in Fig. 1 (a more detailed definition of $T_{M,N}$ is given in Supplementary Material S1).

In the thermodynamic limit, the correlation functions in Eq. (1) can be determined by the maximal eigenvalue Λ_0 and the corresponding left $\langle \psi_{M,N}^l |$ and right $|\psi_{M,N}^r \rangle$ eigenvectors of $T_{M,N}$:

$$\langle O_s(t)O_0(0) \rangle = \frac{\langle \psi_{M,N}^l | \tilde{T}_{M,N}(O_0, O_s) | \psi_{M,N}^r \rangle}{\Lambda_0^{s+1}}. \quad (3)$$

Here $\langle \psi_{M,N}^l | \psi_{M,N}^r \rangle = 1$ is implied and $\tilde{T}_{M,N}(O_0, O_s) \equiv T_{M,N}(O_0) T_{M,N}^{s-1} T_{M,N}(O_s)$ is a product of $s+1$ transfer matrices, where $T_{M,N}(O_j)$ is a modified transfer matrix containing operator O_j at site $j=0$ and s (see Fig. 1).

In order to evaluate the long time correlation function accurately, one needs to understand how the entanglement is built up in the maximal eigenvectors of $T_{M,N}$ during the time evolution. It is instructive to first consider the infinite-temperature case where the thermal density matrix $e^{-\beta H}$ becomes an identity and $T_{M,N}$ associated with its dual eigenvectors $\langle \psi_{M,N}^l |$ and $|\psi_{M,N}^r \rangle$ are reduced to an M -independent matrix T_N associated with $\langle \psi_N^l |$ and $|\psi_N^r \rangle$ (Fig. 2(a)). For the convenience in the discussion below, we use τ_n^* to denote a pair of virtual states $(\tau_n, \bar{\tau}_n)$, $n = 1, \dots, N$, and $|\tau_n^* \rangle = \sum_{\tau_n, \bar{\tau}_n} \delta_{\tau_n, \bar{\tau}_n} |\tau_n, \bar{\tau}_n \rangle$ to denote a maximally entangled state of τ_n and $\bar{\tau}_n$. An important property of T_n , as shown in the supplementary material, is that the contraction of its left maximal

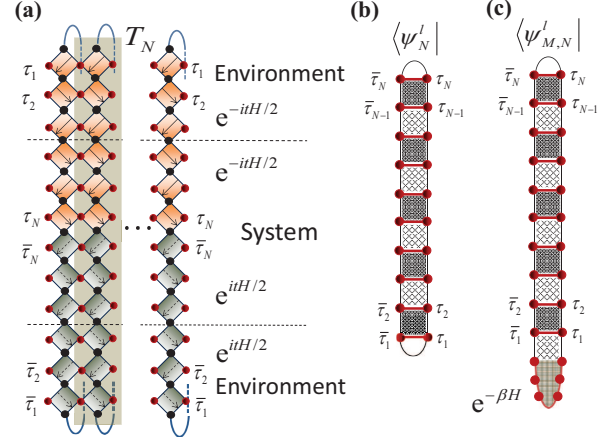


FIG. 2. (Color online) (a) Graphical representation of the transfer matrix T_N . τ_n and $\bar{\tau}_n$ represent the time along the forward and backward evolution directions, respectively. (b) Schematic plot of the entanglement structure for the maximal left eigenvector of T_N . $\langle \psi_N^l |$ is an entangled state of singlet pairs between τ_n and $\bar{\tau}_n$. The two parts separated by a dark shadow has stronger entanglement than that separated by a light shadow. The right maximal eigenvector $|\psi_N^r \rangle$ has a similar entanglement structure with the dark and light shadows interchanged. The new TMRG scheme bi-partitions the QTM into $e^{itH/2} e^{-itH/2}$ and $e^{-itH/2} e^{itH/2}$ such that the maximally entangled pair is locked within each block. (c) The maximal eigenvectors of $T_{M,N}$ at finite temperature have similar structures.

eigenvector $\langle \psi_n^l |$ with $|\tau_n^* \rangle$ satisfies the following equation

$$\langle \psi_n^l | \tau_n^* \rangle = \langle \psi_{n-1}^l | = \langle \psi_{n-2}^l | \langle \tau_{n-1}^* | \quad (4)$$

for an even n . A similar equation holds for the right eigenvector $|\psi_n^r \rangle$ but with odd n . Eq. 4 means that the contraction of the left eigenvector $\langle \psi_n^l |$ with a maximally entangled pair $|\tau_n^* \rangle$ produces another separated maximally entangled pair $|\tau_{n-1}^* \rangle$ if n is even. This implies that the virtual basis states τ_n and $\bar{\tau}_n$ at the same forward and backward real time n have strong tendency to form a singlet pair. Thus the left maximal eigenvector should have an entanglement structure as depicted in Fig. 2(b), where the red bonds denote singlet pair states, and the upper and lower parts separated by a dark (light) shadow have stronger (weaker) entanglement. A similar entanglement structure exists for the right maximal eigenvector $|\psi_n^r \rangle$, but the dark and light shadows are interchanged.

As taking into account the finite temperature effect, the QTM $T_{M,N}$ is obtained by simply adding two blocks of thermal operator at the top and bottom of T_N as shown in Fig. 1. Following the derivation of Eq. (4) (see Supplementary Material S2), we can obtain

$$\langle \psi_{M,n}^l | \tau_n^* \rangle = \langle \psi_{M,n-1}^l | = \langle \psi_{M,n-2}^l | \langle \tau_{n-1}^* | \quad (5)$$

for an even real-time n , and the eigenvector $|\psi_{M,n}^r \rangle$ has a similar property for odd n . Here $\langle \psi_{M,n}^l |$ and $|\psi_{M,n}^r \rangle$

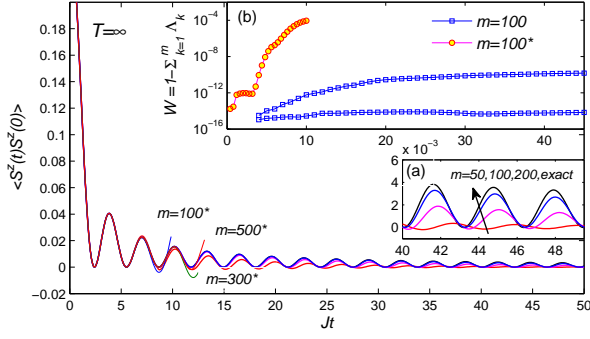


FIG. 3. (Color online) Time-dependent autocorrelation $\langle S^z(t)S^z(0) \rangle$ for the Heisenberg model (6) with $\Delta = 0$ at infinite temperature. m is the number of basis states retained in the calculation. The results The data with m marked by asterisk are obtained by the conventional TMRG scheme. Inset (a): Blow-up of the autocorrelation in the long time region. Inset (b): Comparison of the discarded weight $W = 1 - \sum_{k=1}^m \Lambda_k$ obtained by the BTMRG with that obtained by the conventional TMRG. The two W -curves for our scheme correspond to the cutting boundary through the dark shadow with strong entanglement and through the light shadow with weak entanglement, respectively.

denote the left and right maximal eigenvectors of $T_{M,n}$ with M fixed and $n = 1, \dots, N$. Thus, the eigenvectors of $T_{M,N}$ should have a slower increasing entanglement between the block involving imaginary-time and the block involving real-time. Furthermore, the eigenvectors of $T_{M,N}$ should have a similar entanglement structure for the block involving real-time as the structure of the eigenvectors of T_N (see Fig. 2(c)).

The above discussion suggests that in order to suppress the growth of the entanglement with time evolution, we should redefine T_N on a folded lattice where τ_n and $\bar{\tau}_n$ at real time n are merged into a single site, as shown in Fig. 2(b). For $T_{M,N}$ on a folded lattice, the additional sites τ_m and $\bar{\tau}_m$ for imaginary time are also merged, but the folded block $e^{-\beta H}$ is regarded as a heat bath (Fig. 2(c)). Thus the strong entanglement between τ_N and $\bar{\tau}_N$ is confined within each time step and will not proliferate with time evolution. This can avoid the linear growth problem of entanglement with time in the conventional TMRG schemes[4].

Based on the above argument, we propose to do the BTMRG calculation by collecting a segment of local matrices around the center of the virtual lattice as the system block and the rest of local tensors as the environment block (Fig. 2(a)). In the infinite temperature limit, this is equivalent to dividing the quantum transfer matrix into $e^{itH/2}e^{-itH/2}$ and $e^{-itH/2}e^{itH/2}$ parts. At each iteration, both system and environment blocks are enlarged by adding two different rotated matrices w 's (w^{-1} 's) at the upper (lower) boundary site between the two blocks. For the finite-temperature calculation, we first cool down the temperature to a desired value by taking the imagi-

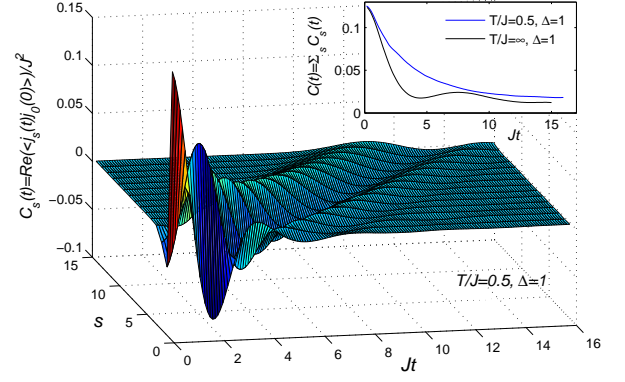


FIG. 4. (Color online) The correlation function $C_s(t)$ for the Heisenberg model with $\Delta = 1$ and $s = 0 - 15$ at $T/J = 0.5$. Inset: Current correlation function $C(t)$ for $\Delta = 1$ at $T/J = 0.5$ and $T = \infty$, respectively.

nary time evolution, and then take the real time evolution by embedding T_M into the environment block. In this case, the system and environment blocks are equivalent to $e^{itH/2}e^{-itH/2}$ and $e^{-itH/2}e^{-\beta H}e^{itH/2}$, respectively.

To test the method, we calculate the longitudinal spin autocorrelation $\langle S^z(t)S^z(0) \rangle$ for the anisotropic spin-1/2 Heisenberg model defined by the Hamiltonian

$$H = \sum_j J(S_j^x S_{j+1}^x + S_j^y S_{j+1}^y + \Delta S_j^z S_{j+1}^z). \quad (6)$$

When $\Delta = 0$, this model is equivalent to the spinless free fermion model where an exact result for the autocorrelation is available [9]. We use the BTMRG to evaluate the maximal eigenvectors of $T_{M,N}$ [8]. By properly choosing the dual biorthonormal bases, the BTMRG can achieve significant improvement of numerical stability over the conventional TMRG.

Fig. 3 compares the results of the autocorrelation for the above model up to $Jt = 50$ with $\delta_t = 0.05$ and $\Delta = 0$ at infinite temperature obtained from both the BTMRG and the conventional TMRG. We find that the time scale that can be reached by the conventional TMRG with reliable accuracy is quite small, due to the fast increase of entanglement entropy with evolving time. However, our BTMRG calculation can reach much longer time scale with high precision. In particular, as shown in Fig. 3(b) the truncation error $W = 1 - \sum_{k=1}^m \Lambda_k$ increases very rapidly with increasing time scale in the TMRG calculation. In contrast, in our BTMRG calculation W saturates asymptotically. This shows that the entanglement builds up mainly between the operators e^{-itH} and e^{itH} . We also calculate the real-time dynamics for several spin-1/2 chains at various temperatures. The results are consistent with our prediction for the entanglement structure at finite temperature and the dynamics can be reliably evaluated on a time scale far longer than the previous TMRG calculations (see the supplementary material).

An advantage of our BTMRG scheme is its competitive accuracy with much cheaper computational cost. The computational cost of the BTMRG scales with the basis states retained as $O(m^3)$, one order less than in the folding algorithm as well as the tDMRG using matrix product states where the computational cost scales as $O(m^4)$. Moreover, our method works directly in the thermodynamic limit and there is no finite lattice size effect. The most challenging problem in our method is the calculation of long distance correlation functions, since it involves a calculation of the product of many transfer matrices $\tilde{T}_{M,N}(O_0, O_s)$ (see Fig. 1).

In our algorithm, this wide transfer matrix $\tilde{T}_{M,N}(O_0, O_s)$ is approximated by a matrix-product operator (MPO) and is updated in a similar way as the evolution of the matrix product state in the modified tDMRG[6] (see the supplementary material). Our method, however, differs from the modified tDMRG in three aspects: (i) The infinite-length MPO used in tDMRG for the correlator is replaced by a $(s+1)$ -length MPO representing the transfer matrix $\tilde{T}_{M,N}(O_0, O_s)$. This leads to dramatic reduction of computational storage and time. (ii) The left (right) bond of the first (last) MPO matrix is obtained by projecting the matrix from the left (right) onto the reduced basis states describing the left (right) maximal eigenvector. Since the number of state kept, m , is usually small due to our special bi-partitioning scheme, the bond dimension χ of the MPO matrices is typically smaller than that in tDMRG. (iii) The correlator is obtained by contracting the $(s+1)$ -length MPO with the left and right maximal eigenvectors at the left and right bonds respectively. These advantages can be seen from the calculation of the current-current correlation function[6, 10]

$$C_s(t) = \langle j_s(t) j_0(0) \rangle, \quad (7)$$

where $j_s = -\frac{iJ}{2}(S_s^+ S_{s+1}^- - S_{s+1}^+ S_s^-)$. The long time limit of $C(t) = \sum_s C_s(t)$ gives the value of Drude weight. Fig. 4 shows $C_s(t)$ for the Heisenberg model (6) with $\Delta = 1$ and $s = 0-15$ at $T/J = 0.5$. The result is obtained by fixing the truncation error less than $W = 1 \times 10^{-11}$ for the maximal eigenvectors (the number of basis states is typically around $m = 250$) and less than $W = 1 \times 10^{-6}$ for the evolution of matrix product operators with the bond dimension around $\chi = 500$. The figure clearly shows that the large distance and long-time dynamics can be accurately determined. Another notable advantage of our method is that in the determination of these correlation functions, the left and right maximal eigenvectors need to be evaluated just once. The inset of Fig. 4 shows the spatial integrated current correlation function $C(t)$ up to time scale where $C(t)$ saturates for $\Delta = 1$ at $T/J = 0.5$ and $T = \infty$, which agree well with the results given in

Refs. 6 and 10.

To summarize, we identify the entanglement structure of the maximal eigenvectors of the QTM proposed in [7]. It reveals the origin of the entanglement growth during the time evolution and the reason why the recent algorithms work [5, 6]. On the basis of this picture, we propose an alternative method based on the BTMRG approach by bi-partitioning the system and the environment blocks according to the entanglement structure. Our approach provides an very efficient tool for studying finite-temperature dynamics of 1D quantum lattice models.

Y.-K.H. acknowledges the support by NSC in Taiwan through Grants No. 101-2112-M-232-001.

* ykln@mail.nju.edu.tw

† pcchen@phys.nthu.edu.tw

‡ yjkao@phys.ntu.edu.tw

§ txiang@iphy.ac.cn

- [1] S. R. White, *Phys. Rev. Lett.* **69**, 2863 (1992).
- [2] G. Vidal, *Phys. Rev. Lett.* **91**, 147902 (2003);
S. R. White and A. E. Feiguin, *Phys. Rev. Lett.* **93**, 076401 (2004);
G. Vidal, *Phys. Rev. Lett.* **99**, 220405 (2007).
- [3] A. E. Feiguin and S. R. White, *Phys. Rev. B* **72**, 220401 (2005);
T. Barthel, U. Schollwöck, and S. R. White, *Phys. Rev. B* **79**, 245101 (2009);
T. Nishino, *Journal of the Physical Society of Japan* **64**, 3598 (1995);
R. J. Bursill, T. Xiang, and G. A. Gehring, *Journal of Physics: Condensed Matter* **8**, L583 (1996);
X. Wang and T. Xiang, *Phys. Rev. B* **56**, 5061 (1997);
N. Shibata, *Journal of the Physical Society of Japan* **66**, 2221 (1997).
- [4] J. Sirker and A. Klümper, *Phys. Rev. B* **71**, 241101 (2005).
- [5] M. C. Bañuls, M. B. Hastings, F. Verstraete, and J. I. Cirac, *Phys. Rev. Lett.* **102**, 240603 (2009);
A. Müller-Hermes, J. I. Cirac, and M. C. Bañuls, *New J. Phys.* **14**, 075003 (2012).
- [6] C. Karrasch, J. H. Bardarson, and J. E. Moore, *Phys. Rev. Lett.* **108**, 227206 (2012);
T. Barthel, U. Schollwöck, and S. Sachdev, (2012), [arXiv:1212.3570 \[cond-mat\]](#).
- [7] J. Sirker and A. Klümper, *EPL (Europhysics Letters)* **60**, 262 (2002).
- [8] Y.-K. Huang, *Phys. Rev. E* **83**, 036702 (2011);
Journal of Statistical Mechanics: Theory and Experiment **2011**, P07;
Y.-K. Huang, P. Chen, and Y.-J. Kao, *Phys. Rev. B* **86**, 235102 (2012).
- [9] T. Niemeijer, *Physica* **36**, 377 (1967).
- [10] J. Sirker, R. G. Pereira, and I. Affleck, *Phys. Rev. Lett.* **103**, 216602 (2009);
Phys. Rev. B **83**, 035115 (2011);
S. Jesenko and M. Znidaric, *Phys. Rev. B* **84**, 174438 (2011).

Supplementary Material for “Long-time dynamics of quantum chains: transfer-matrix renormalization group and entanglement of the maximal eigenvector”

Yu-Kun Huang,¹ Pochung Chen,² Ying-Jer Kao,³ and Tao Xiang⁴

¹Graduate School of Engineering Science and Technology,
Nan Jeon University of Science and Technology, Tainan 73746, Taiwan

²Department of Physics and Frontier Research Center on Fundamental and Applied Sciences of Matters,
National Tsing Hua University, Hsinchu 30013, Taiwan

³Department of Physics and Center for Advanced Study of Theoretical Science,
National Taiwan University, No. 1, Sec. 4, Roosevelt Rd., Taipei 10607, Taiwan

⁴Institute of Physics, Chinese Academy of Sciences, P.O. Box 603, Beijing 100190, China
(Dated: May 30, 2018)

S1. DEFINITION OF QUANTUM TRANSFER MATRIX

It is well-known that the standard quantum-to-classical mapping is the Trotter-Suzuki decomposition which decomposes the thermal statistical operator $e^{-1/TH}$ of a one-dimensional (1D) quantum system with Hamiltonian $H = \sum_{j=1}^L h_{j,j+1}$ into a 2D tensor network showing a checkerboard structure. Here T indicates the temperature. As shown in Fig. 1(a), this tensor network can be expressed as a product of local transfer matrices $\nu \equiv e^{-\varepsilon h_{j,j+1}}$ with matrix element

$$\nu_{k,k+1}^{j,j+1} = \left\langle \sigma_{k+1}^j \sigma_{k+1}^{j+1} \left| e^{-\varepsilon h_{j,j+1}} \right| \sigma_k^j \sigma_k^{j+1} \right\rangle, \quad (1)$$

where $\varepsilon = 1/MT$ is the imaginary-time step and M the Trotter number in the imaginary-time direction. The subscripts j and k represent the physical site (represented graphically by full black circles) coordinates in the spatial and imaginary-time directions, respectively. This mapping has several disadvantages. The obvious one, for example, is that the quantum transfer matrix (QTM) is two columns wide, leading to more memory space and computational complexity. A more detailed discussions of its disadvantages can be found in Ref. [1]. In this work, we employ an alternative quantum-to-classical mapping proposed in Ref. [1] which decomposes the operator $e^{-1/TH}$ into $e^{-1/TH} \approx \lim_{M \rightarrow \infty} \{T_1(\varepsilon) T_2(\varepsilon)\}^{M/2}$ where $T_{1,2}(\varepsilon) = T_{R,L} e^{-\varepsilon H}$ and $T_R = e^{iP}$ ($T_L = e^{-iP}$), with P being the momentum operator, denotes the right (left) shift operator. The resulting 2D tensor network has alternating rows and additional virtual (auxiliary) sites (represented graphically by full red circles) as shown in Fig. 1(b), where $T_1(\varepsilon)$ ($T_2(\varepsilon)$) is a row-to-row transfer matrix which is composed of a 45° clockwise (counter-clockwise) rotation of the local matrix ν and a one column wide QTM as indicated by a shaded rectangle can be defined. Instead of acting on a chain of physical sites in the time direction as in the Trotter-Suzuki decomposition, this QTM acts on a chain of virtual sites in the time direction. Such a mapping arises in the context of exactly solvable model at finite temperature [2] and Sirker [3] has

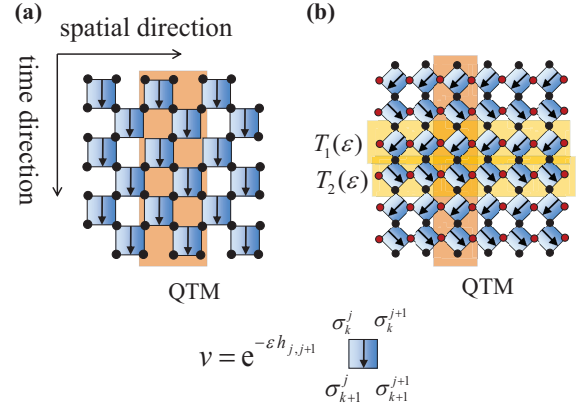


FIG. 1. (Color online) (a) From standard Trotter-Suzuki decomposition of the operator $e^{-1/TH}$, one can define a two-column wide QTM. (b) The mapping proposed in Ref. [1] maps $e^{-1/TH}$ onto a tensor network with alternating rows and additional sites in an auxiliary mathematical space where one can define a one-column wide QTM.

proved that this mapping has a second-order error correction term and can be generally applied to 1D systems with nearest neighbor interactions.

When considering the time-dependent correlation function as in Eq. (1) in the main article, a similar decomposition can be applied to the time-evolution operators e^{-itH} and e^{itH} , with ν being replaced by complex local matrices $w \equiv e^{-i\delta_t h_{j,j+1}}$ and $w^{-1} \equiv e^{i\delta_t h_{j,j+1}}$ respectively, and ε being replaced by the real-time step $\delta_t = t/N$ where N denotes the Trotter number in the real-time direction. These additional decompositions results in a 2D tensor network as shown in Fig. 2 where a new QTM $T_{M,N}$ can be defined. Due to the trace operation in Eq. (1) in the main article, we note that this tensor network has a periodic boundary condition at the top and bottom physical sites and an additional transfer matrix $\tilde{T}_{M,N}(O_0, O_s) \equiv T_{M,N}(O_0) T_{M,N}^{s-1} T_{M,N}(O_s)$ as shown in Fig. 2 is involved, where $T_{M,N}(O_j)$ is a modified transfer matrix containing operator O_j at site $j = 0$ and s .

In the thermodynamic limit, the calculation of the dy-

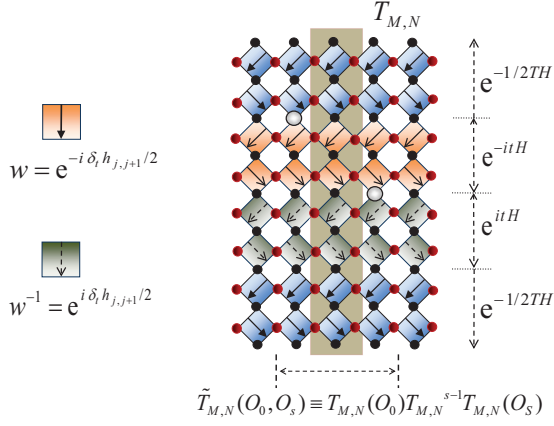


FIG. 2. (Color online) The alternative quantum-to-classical mapping decomposes the operator $e^{itH}e^{-itH}e^{-1/TH}$ of a 1D quantum system into a 2D tensor network where a QTM $T_{M,N}$ can be defined. The two-point dynamic correlation function involves a modified transfer matrix $\tilde{T}_{M,N}(O_0, O_s)$ where the two observables at different site and different time are represented graphically by two empty circles.

dynamic correlation function can be recast into Eq. (3) in the main article. As a result, two main issues concerning the transfer-matrix renormalization group (TMRG) calculation of the long-time dynamics for this correlator arise: the identification of the entanglement structure of the maximal eigenvectors for the $T_{M,N}$ and the efficient evaluation of the additional transfer matrix $\tilde{T}_{M,N}(O_0, O_s)$ especially when the distance s is large. In the following, we shall discuss in details how to tackle these two issues respectively.

S2. ENTANGLEMENT STRUCTURE OF THE MAXIMAL EIGENVECTOR

Let us first consider the case $T = \infty$ ($e^{-1/TH} = 1$). Through the quantum-to-classical mapping, the operator $e^{itH}e^{-itH}$ can be decomposed into a 2D tensor network where a M -independent QTM T_N can be defined, which is shown in Fig. 3. The discovery of the entanglement structure of the maximal eigenvectors of T_N provides us not only the understanding that how the entanglement builds up in conventional TMRG calculation but also a picture that how the entanglement growth can be avoided by taking a different bi-partitioning scheme for the QTM T_N . In this section, we will prove three important properties of T_N , from which one can identify the entanglement structure of the maximal eigenvectors of T_N as described in the main article. Assume the dimension of the local Hilbert space is d . Let τ_n^* denote a pair of virtual states $(\tau_n, \bar{\tau}_n)$ at the same forward and backward real-time n , $n = 1, \dots, N$, $|\tau_n^*\rangle = \sum_{\tau_n, \bar{\tau}_n} \delta_{\tau_n, \bar{\tau}_n} |\tau_n, \bar{\tau}_n\rangle$ a maximally en-

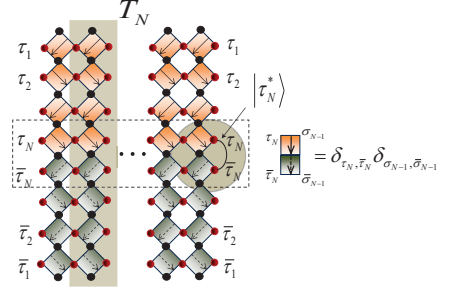


FIG. 3. (Color online) By contracting T_N^L with $|\tau_N^*\rangle$ from the right, we have a tensor product of $|\tau_N^*\rangle$ on the left and T_{N-1}^L , which can be expressed as $T_N^L |\tau_N^*\rangle = |\tau_N^*\rangle T_{N-1}^L$.

tangled state of τ_n and $\bar{\tau}_n$, and $\langle \psi_n^l |$ and $|\psi_n^r\rangle$ the left and right maximal eigenvectors of T_n respectively. These properties are based on a key observation as indicated in Fig. 3. For an arbitrary L , contracting T_N^L with $|\tau_N^*\rangle$ from the right, the two matrices w and w^{-1} enclosed in the shadow circle contract to an identity. Thus, two physical sites (σ_{N-1} and $\bar{\sigma}_{N-1}$) contract and two virtual sites (τ_N and $\bar{\tau}_N$) at the left hand side contract such that the left-adjacent matrices w and w^{-1} connects and become an identity again. This process can continue from right to left through the QTM, and finally we obtain a separated maximally entangled pair state $|\tau_N^*\rangle$ on the left. Two rows of local matrices, enclosed by the dashed rectangle in Fig. 3, contract to identities and a QTM T_{N-1}^L with one fewer Trotter number is formed. This can be expressed as $T_N^L |\tau_N^*\rangle = |\tau_N^*\rangle T_{N-1}^L$.

1. The maximal eigenvalue Λ_0 of T_N is d irrespective of the Trotter number N , i.e.,

$$\Lambda_0 = d. \quad (2)$$

proof: It is straightforward to show that, as $L \rightarrow \infty$, $\Lambda_0^L = \text{Tr}(T_N^L) = \text{Tr}(e^{itH}e^{-itH}) = d^L$. Consequently, $\Lambda_0 = d$ irrespective of the Trotter number N . Furthermore, in the thermodynamic limit, one has

$$\lim_{L \rightarrow \infty} T_n^L = d^L |\psi_n^r\rangle \langle \psi_n^l|, \quad (3)$$

for arbitrary n . Here the normalization condition $\langle \psi_n^l | \psi_n^r \rangle = 1$ is used.

2. For all even n , the right eigenvector $|\psi_n^r\rangle$ is related to the eigenvector $|\psi_{n-1}^r\rangle$ by

$$|\psi_n^r\rangle = |\tau_n^*\rangle |\psi_{n-1}^r\rangle. \quad (4)$$

proof: The key observation in Fig. 3 is a recurrence relation. It satisfies the relation

$$T_n^L |\tau_n^*\rangle = |\tau_n^*\rangle T_{n-1}^L, \quad (5)$$

for all even Trotter number n and arbitrary L . Therefore, one has

$$\begin{aligned} T_n^L |\tau_n^*\rangle |\psi_{n-1}^r\rangle \\ = |\tau_n^*\rangle T_{n-1}^L |\psi_{n-1}^r\rangle = d^L |\tau_n^*\rangle |\psi_{n-1}^r\rangle. \end{aligned} \quad (6)$$

Accordingly, $|\tau_n^*\rangle |\psi_{n-1}^r\rangle$ is a right eigenvector of T_n with eigenvalue d . Since d is always the maximal eigenvalue of T_n , one obtains the property (2) of the QTM T_N .

3. For all even n , by contracting the left eigenvector $\langle\psi_n^l|$ with $|\tau_n^*\rangle$, we have

$$\langle\psi_n^l|\tau_n^*\rangle = \langle\psi_{n-1}^l| = \langle\psi_{n-2}^l|\tau_{n-1}^*|, \quad (7)$$

and the eigenvector $|\psi_{n-1}^r\rangle$ has a similar property.

proof: As $L \rightarrow \infty$, from $T_n^L |\tau_n^*\rangle = |\tau_n^*\rangle T_{n-1}^L$ and $T_{n-1}^L = d^L |\psi_{n-1}^r\rangle \langle\psi_{n-1}^l|$, one obtains

$$T_n^L |\tau_n^*\rangle = d^L |\tau_n^*\rangle |\psi_{n-1}^r\rangle \langle\psi_{n-1}^l|. \quad (8)$$

Similarly, from $T_n^L |\tau_n^*\rangle = d^L |\psi_n^r\rangle \langle\psi_n^l|\tau_n^*\rangle$ and Eq. (4), one obtains

$$T_n^L |\tau_n^*\rangle = d^L |\tau_n^*\rangle |\psi_{n-1}^r\rangle \langle\psi_n^l|\tau_n^*\rangle. \quad (9)$$

By comparing Eq. (8) with Eq. (9), we conclude that

$$\langle\psi_n^l|\tau_n^*\rangle = \langle\psi_{n-1}^l|. \quad (10)$$

It is easy to see that, however, T_{n-1}^L has the same structure as T_n^L , with the roles of left and right eigenvectors interchange with each other. Consequently, one has

$$\langle\psi_{n-1}^l| = \langle\psi_{n-2}^l|\tau_{n-1}^*| \quad (11)$$

according to Eq. (4). Similarly, because T_{n-1}^L has the same structure as T_n^L , all the argument applying to $\langle\psi_n^l|$ also apply to $|\psi_{n-1}^r\rangle$. This is exactly the property (3) of the QTM T_N .

From these properties, we argue that the maximal eigenvectors of T_N have an entanglement structure as depicted in Fig. 2(b) in the main article.

As taking into account the finite-temperature effect, the QTM $T_{M,N}$ is obtained by adding two blocks of thermal operator at the top and bottom of T_N as shown in Fig. 2. Similar to the derivation of Eq. (2), it is easy to obtain

$$\Lambda_0 = \rho_M, \quad (12)$$

where ρ_M denotes the maximal eigenvalue of QTM T_M involving only imaginary-time. Meanwhile, since the key observation in Fig. 3 still hold for the finite-temperature

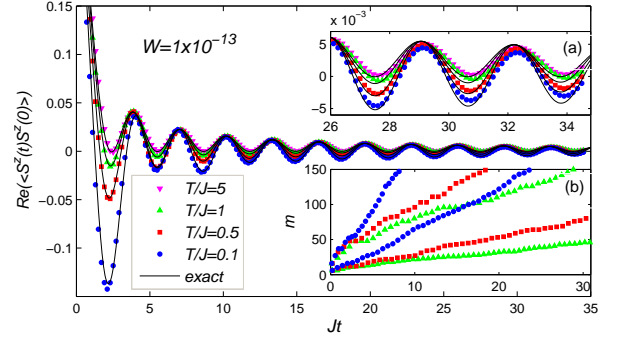


FIG. 4. (Color online) Autocorrelation $\text{Re}(\langle S^z(t)S^z(0) \rangle)$ of XXZ chain at various temperatures. Inset (a): Blow-up of the $\text{Re}(\langle S^z(t)S^z(0) \rangle)$ near the large time-scale region. Inset (b): The number of keeping states under fixed discarded weight $W = 10^{-13}$ increases linearly.

case, i.e., $T_{M,N}^L |\tau_N^*\rangle = |\tau_N^*\rangle T_{M,N-1}^L$. Following the above derivation, for the maximal eigenvectors at finite temperature, it can also be obtained

$$\langle\psi_{M,n}^l|\tau_n^*\rangle = \langle\psi_{M,n-1}^l| = \langle\psi_{M,n-2}^l|\tau_{n-1}^*| \quad (13)$$

for an even real-time Trotter number n , and the eigenvector $|\psi_{M,n}^r\rangle$ has a similar property for odd n . Here $\langle\psi_{M,n}^l|$ and $|\psi_{M,n}^r\rangle$ denote the left and right maximal eigenvectors of $T_{M,n}$ with M fixed and $n = 1, \dots, N$. Thus, we assert that the eigenvectors of $T_{M,N}$ have a slower increasing entanglement between the block involving imaginary-time and the block involving real-time. Furthermore, the eigenvectors of $T_{M,N}$ have a similar entanglement structure for the block involving real-time as the structure of the eigenvectors of T_N as shown in Fig. 2(c) in the main article.

S3. REAL-TIME DYNAMICS AT FINITE AND ZERO TEMPERATURE

Here we show our results for the spin-1/2 XXZ chain for $\Delta = 0$ at various finite temperatures. In Fig. 4 we plot the longitudinal spin autocorrelation function $\text{Re}(\langle S^z(t)S^z(0) \rangle)$ as a function of time at temperatures $T/J = 5, 1, 0.5$, and 0.1 respectively. In the inset Fig. 4(a) we zoom in the large time regime. It is clear that the results are still very accurate at large time. In the inset Fig. 4(b) we plot the time-dependent number of keeping states m , under fixed discarded weight $W = 1 \times 10^{-13}$. It shows a linear, instead of exponential, growth with time. For each temperature, there are two time-dependent m -lines corresponding to the cut through the dark and light shadows respectively. Furthermore, we find that the number m increases faster with time when the temperature decreases. These results are consistent with our prediction of the entanglement structure for the

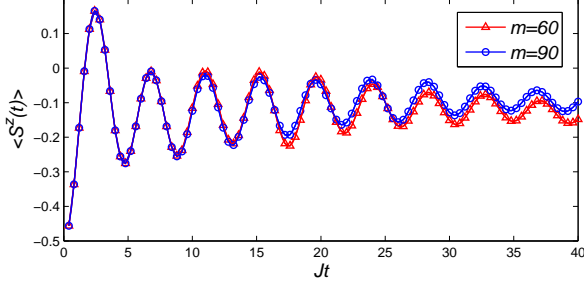


FIG. 5. (Color online) Time-dependent magnetization of an XY chain at zero temperature with initial state $|0\rangle = |\downarrow\rangle^{\otimes L}$. Here, the time scale should be divided by a factor of 4 to be comparable to Fig. 12 in [4].

maximal eigenvectors at finite temperatures. As shown in the figure, we successfully reach time scale $Jt = 35$ or more.

Our BTMRG scheme can also be applied to calculate the long-time dynamics of quantum chains for pure states at zero-temperature. In this case, the upper and lower boundary of the 2D tensor network (see Fig. 2(a) in the main article) is restricted to fixed boundary conditions, i.e., contracting the pure state at the upper and lower boundary of the network. As an example, we calculate the time-evolution of magnetization per site $\langle S^z(t) \rangle$ of an XY model at zero temperature with initial state $|0\rangle = |\downarrow\rangle^{\otimes L}$. The Hamiltonian reads

$$H = \sum_j J(S_j^x S_{j+1}^x - \frac{1}{2} S_j^y S_{j+1}^y). \quad (14)$$

The results with $m = 60, 90$ are shown in Fig. 5. Our results are comparable with the results obtained by the folding algorithm (see Fig. 12 in [4], with caution that our time scale should be divided by a factor of 4 to be comparable to their definition of Hamiltonian).

S4. COMPARISON BETWEEN OUR BTMRG METHOD AND THE MODIFIED TDMRG METHOD

In this section, we provide details in dealing with the issue of efficient evaluation of the large distance correlation function. Some comparisons between our BTMRG method and the modified tDMRG method proposed in Ref. [5] are also given.

In BTMRG framework, apart from the evaluation of the maximal eigenvalue Λ_0 and the associated dual eigenvectors $|\psi^l\rangle$ and $|\psi^r\rangle$, the correlator as in Eq. (3) in the main article involves the evaluation of the modified transfer matrix $\tilde{T}_{M,N}(O_0, O_s)$ (see Fig. 2).

For autocorrelation function $\langle S^z(t) S^z(0) \rangle$ as shown in Fig. 4, this additional transfer matrix is only one-column

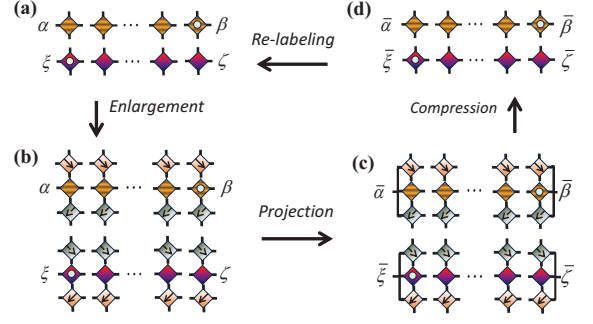


FIG. 6. (Color online) Main steps of renormalization group for $\tilde{T}_{M,N}(O_0, O_s)$. (a) MPO representation of the system and environment blocks. The vertical indices are the analogy of the physical quantum state and ancilla state in recent tDMRG algorithm. $\{|\alpha\rangle\}$ and $\{|\beta\rangle\}$ ($\{|\xi\rangle\}$ and $\{|\zeta\rangle\}$) represent the dual biorthonormal bases in describing the left $|\psi^l\rangle$ and right $|\psi^r\rangle$ dominant eigenstates for system (environment) block. (b) Enlarging MPO matrices by adding $w = e^{-i\delta_t h_{j,j+1}}$ and $w^{-1} = e^{i\delta_t h_{j,j+1}}$ in between the system and environment blocks. This process is equivalent to the main feature of tDMRG: evolving the quantum state with ancilla state evolved in reverse time. (c) Projecting the first and last enlarged MPO matrices from the left and right onto the new biorthonormal basis states $\{|\bar{\alpha}\rangle\}$ and $\{|\bar{\beta}\rangle\}$ ($\{|\bar{\xi}\rangle\}$ and $\{|\bar{\zeta}\rangle\}$) for the enlarged system (environment) block obtained through BTMRG. (d) Compressing the MPO by carrying out SVD and truncation on each bond of the MPO. The correlation function is obtained by contracting the MPOs with $|\psi^l\rangle$ and $|\psi^r\rangle$ at the left and right bonds of the MPOs.

wide. The correlator can be easily obtained by splitting $\tilde{T}_{M,N}(S^z, S^z)$ into system and environment blocks, enlarging both blocks, and projecting both blocks onto the dual reduced biorthonormal bases describing the left $|\psi^l\rangle$ and right $|\psi^r\rangle$ maximal eigenvectors, just as in the same way of the treatment for the QTM $T_{M,N}$. However, in certain cases, one has to calculate correlation function for two operators far distance away. It is a challenge for BTMRG to evaluate large-distance correlators since it involves the evaluation of a wide transfer matrix $\tilde{T}_{M,N}(O_0, O_s)$. Here, by approximating $\tilde{T}_{M,N}(O_0, O_s)$ as a matrix-product operator (MPO) and renormalizing the MPO matrices in a similar way as renormalizing the QTM $T_{M,N}$, we succeed to calculate the correlator very efficiently for large distance s . In particular, we show that our BTMRG is equivalent to a novel tDMRG algorithm exactly in the thermodynamic limit.

In Fig. 6 we sketch the main renormalization group (RG) steps for the transfer matrix $\tilde{T}_{M,N}(O_0, O_s)$ within BTMRG framework. In each step, the transfer matrix $\tilde{T}_{M,N}(O_0, O_s)$ is split into the system (the upper) and environment (the lower) blocks according to our special bi-partitioning configuration. Each block is expressed as a $(s+1)$ -length MPO, where each column of the block is represented as a local tensor (MPO matrix) with two ver-

tical indices labelling site basis states and two horizontal indices labelling bond states between the MPO matrices.

We start from Fig. 6(a) where the left and right maximal eigenvectors can be expressed in terms of the dual biorthonormal bases $\{|\alpha\rangle\}$ and $\{|\beta\rangle\}$ ($\{|\xi\rangle\}$ and $\{|\zeta\rangle\}$) for the system (environment) block. The next step (Fig. 6(b)) is to enlarge every MPO matrix by adding local matrices $w = e^{-i\delta_\tau h_{j,j+1}}$ and $w^{-1} = e^{i\delta_\tau h_{j,j+1}}$ in between the system and environment blocks. These two 45° -rotations of w and w^{-1} alternate in the clockwise and counter-clockwise manner for every two RG iterations.

In the mean time, on the other hand, the QTM $T_{M,N}$ undergoes the same process and the new reduced dual biorthonormal bases $\{|\bar{\alpha}\rangle\}$ and $\{|\bar{\beta}\rangle\}$ ($\{|\bar{\xi}\rangle\}$ and $\{|\bar{\zeta}\rangle\}$) for the enlarged system (environment) block are obtained through BTMRG method [6]. Then, we first project the first and last enlarged MPO matrices from the left and right onto the new basis states respectively (Fig. 6(c)), and subsequently compress the MPO by carrying out singular-value decomposition (SVD), keeping the χ most relevant states, and truncating the other irrelevant states on each bond of the MPO (Fig. 6(d)). As a consequence, the dynamic correlator is evaluated by contracting the MPOs with the left $|\psi^l\rangle$ and right $|\psi^r\rangle$ maximal eigenvectors at the left and right bonds of the MPOs. This completes a cycle of the RG steps and the next cycle is repeated by re-labelling the biorthonormal basis state: $\bar{\alpha} \rightarrow \alpha$, $\bar{\beta} \rightarrow \beta$, $\bar{\xi} \rightarrow \xi$, and $\bar{\zeta} \rightarrow \zeta$ until the desired time scale is reached.

We particularly note that the vertical indices of the MPO in our BTMRG are the analogy of the physical quantum state and ancilla state in recent tDMRG algorithm [5]. The process in step (b) is completely equivalent to the main feature of tDMRG: evolving the quantum state with ancilla state evolved in reverse time. Since tDMRG merely works with finite system, our BTMRG algorithm can thus be regarded as a novel tDMRG al-

gorithm exactly in the thermodynamic limit. The most notable advantages of our BTMRG over tDMRG are: (i) the infinite-length MPO in tDMRG is reduced to a $(s+1)$ -length MPO leading to dramatic saving of memory space and computing time; (ii) the left (right) bond of the first (last) MPO matrix of our BTMRG is obtained by projecting the MPO matrices from the left (right) onto the new reduced basis states. Since the number m of reduced basis states is small (see Fig. 4), the bond dimension χ of the MPO is thus smaller than that of tDMRG; and (iii) the dynamic correlator is obtained by contracting the $(s+1)$ -length MPO with the left and right maximal eigenvectors at the left and right bonds respectively. In cases when one has to calculate correlation functions for various distances, this advantage is particularly significant because the left and right eigenvectors only need to be calculated once while the MPS-evolution in tDMRG must be performed from the beginning for each correlation function.

-
- [1] J. Sirker and A. Klümper, EPL (Europhysics Letters) **60**, 262 (2002).
 - [2] A. Klümper, in *Quantum Magnetism*, Lecture Notes in Physics, Vol. 645 (Springer Berlin / Heidelberg, 2004) pp. 349–379.
 - [3] J. Sirker, *Transfer matrix approach to thermodynamics and dynamics of one-dimensional quantum systems*, Ph.D. thesis, Universität Dortmund (2002).
 - [4] A. Müller-Hermes, J. I. Cirac, and M. C. Bañuls, New J. Phys. **14**, 075003 (2012).
 - [5] C. Karrasch, J. H. Bardarson, and J. E. Moore, Phys. Rev. Lett. **108**, 227206 (2012); T. Barthel, U. Schollwöck, and S. Sachdev, (2012), arXiv:1212.3570 [cond-mat].
 - [6] Y.-K. Huang, Phys. Rev. E **83**, 036702 (2011); Journal of Statistical Mechanics: Theory and Experiment **2011**, P070; Y.-K. Huang, P. Chen, and Y.-J. Kao, Phys. Rev. B **86**, 235102 (2012).